Structure–property relationships in styrene–butyl acrylate emulsion copolymers: 1. Preparation and characterization of latexes

A. Cruz-Rivera and L. Rios-Guerrero
Facultad de Quimica, UNAM, 04510 Mexico DF, Mexico

and C. Monnet, B. Schlund, J. Guillot and C. Pichot*
LMO-CNRS, BP 24, 69390 Vernaison, France
(Received 11 October 1988; accepted 16 January 1989)

In order to prepare model systems for investigating structure–property relationships, a series of butyl acrylate (BuA)–styrene (S) copolymer latexes were obtained by emulsion copolymerization in the presence of a blend of emulsifiers (Aerosol MA80 + Aerosol 22N) and with $K_2S_2O_8$ as initiator. Three different comonomer compositions were selected (25/75, 50/50 and 75/25) and three reaction pathways (corrected batch, core–shell and multistep polymerizations) were carried out so as to get various particle morphologies. The kinetics of the different copolymerizations were predicted quite correctly using a simple simulation program based on available reactivity ratios r_{ij} and thermodynamic parameters (partition coefficients) as well as on given 'on-line' data (rate of monomer addition). All samples were accurately characterized in terms of molecular properties (molecular-weight distribution, glass transition temperature and chemical microstructure) and colloidal properties (particle size and charge density). Differences can be explained according to the reaction pathway. Extended simulation was also able to predict the corresponding variations in the monomer sequence distributions and glass transition temperatures.

(Keywords: styrene–butyl acrylate copolymer latexes; reaction pathway; kinetics; molecular and colloidal properties; simulation)

INTRODUCTION

Styrene (S)–butyl acrylate (BuA) emulsion copolymers provide an important class of materials used in many industrial applications thanks to the possibility of obtaining a large number of polymer products through the variation of the copolymer composition and the polymerization process. Such a system is quite interesting because of the differences in the physicochemical properties of the monomers (polarity, water solubility) and of the corresponding homopolymers (glass transition temperature, solubility parameters, etc.). Kinetic studies on that system showed that the reactivity ratios determined under batch emulsion conditions[1–3] are close to those obtained in bulk or solution polymerization[4,5], but somewhat different from those corresponding to semicontinuous conditions[6]. Moreover, it was found that, due to the relatively higher water solubility of BuA ($1.2\,g\,l^{-1}$ for BuA, and $0.3\,g\,l^{-1}$ for styrene at 70°C), the formation of particles is largely dominated by a homogeneous nucleation mechanism, except when the emulsifier concentration exceeds its critical micelle concentration (c.m.c.)[7].

In the past decade, numerous work and patents have described the preparation of structured latexes by multistep emulsion polymerization; many parameters were found to interfere in the control of the particle morphology and have been recently reviewed[8,9]. Pioneering studies by Matsumoto *et al.*[10,11] clearly showed that the sequence of addition of the second monomer could affect the final particle morphology, according to its relative hydrophilicity with respect to that of the polymer constituting the seed. More recent works provide information on the core–shell polymerization mechanism[12] as well as on the main variables controlling the particle morphology in PBuA/PS core–shell latexes using PBuA as the seed. This binary system is quite interesting since the more hydrophobic monomer is stage polymerized onto a PBuA seed, which results in complex particle morphology depending upon the polymerization pathway and degree of grafting reaction between growing PS chains and seed polymer[13].

Many methods have been investigated in order to examine particle structure in these latexes, the direct analysis by transmission electron microscopy becoming more efficient owing to the development of selective staining methods and freeze–fracture techniques. However, dynamic mechanical spectroscopy was found to be a very useful indirect method for determining the particle morphology[14]. This was clearly demonstrated in the case of several recent works: acrylonitrile–styrene/PS (seed) latexes[15] and polystyrene/PBuA (seed) core–shell polymers[16]; in the latter case, phase separation within the particles was initially explained considering three important factors: the seed particle size, seed crosslinking and S/PBuA ratio.

* To whom correspondence should be addressed

0032-3861/89/101872-11$03.00

Up to now, no systematic studies have been reported on the synthesis–structure–property relationships on styrene–butyl acrylate emulsion polymers notably: (i) on two-stage emulsion products using PS as the seed, (ii) on homogeneous latex copolymers derived from adapted polymerization processes. The main purpose of this work is to provide precise information concerning the effect of particle mophology on the thermal and mechanical properties of the corresponding films. In this first paper, it is intended to present typical experimental data on the synthesis as well as on the molecular and colloidal characteristics of a series of styrene–butyl acrylate emulsion copolymers with various combinations of composition and morphology; in addition, simulation programs were applied to predict the kinetic, microstructure and glass transition behaviour of the copolymers as a function of the monomer feed composition and polymerization pathway.

EXPERIMENTAL PROCEDURES

Materials

The monomers, styrene (from Prolabo) and butyl acrylate (from Norsolor), were commercial products and vacuum distilled; they were stored at −5°C under nitrogen. Potassium persulphate (from Merck, 99%) and sodium hydrogen carbonate (from Prolabo, 99.5%) were used as received. Aerosol MA80 (sodium dihexylsulphosuccinate) and Aerosol 22N (tetrasodium n-(1,2-dicarboxyethyl)-n-octadecylsulphosuccinate) (from Cyanamid) were used as emulsifiers; some of their properties are summed up in *Table 1*. Deionized water was purged with N_2 for an hour before use.

Preparation of latexes

Three series of latexes, each one with three different compositions, were prepared according to three copolymerization processes either in one step (composition controlled) or in several steps (core–shell and multilayer polymerization). The device employed was constituted of: (i) a two-litre steel-bottomed reactor vessel equipped with a steel paddle-type stirrer, rotating at 250 rpm, nitrogen inlet, a temperature control and sampling tube; (ii) a titrating pump (Perfusor type) which allows the addition of monomers at a controlled rate.

Composition-controlled copolymerization (*CC*). This was carried out in order to prepare copolymer latexes with homogeneous composition; this is achieved by starting the reaction with the less reactive monomer (BuA) and the calculated amount of the second monomer (S) corresponding to the desired copolymer. The stepwise addition of the remaining S is controlled so as to keep constant the molar ratio of the two monomers; this is done through on-line analysis of unreacted monomers by gas chromatography[17].

Core–shell copolymerization (*CS*). This was a two-step process: first, a polystyrene seed latex was prepared batchwise with the required amount of emulsifier in order to obtain the maximal surface coverage of the particles at 100% conversion; secondly, a buffer and one half of the initiator were charged, and then, after thermal equilibrium, the monomer mixture was added at a rate lower than the maximal polymerization rate (corresponding to maximal particle swelling assuming constant particle number). The remaining initiator was charged after 6 h of reaction so as to reach final conversion near 100%. In some cases, it was necessary to add more emulsifier in order to ensure a better stability of the latex.

Multistage polymerization (*ML*). This was performed, as described above, with only two main differences: the comonomer mixture in the second stage was richer in S, and pure butyl acrylate was introduced in the third step so that the overall composition of the two layers was similar to the composition of the shell obtained in the second process.

Recipes are summarized later in *Tables 3* and *4* for the seed latex and the three series of styrene–butyl acrylate latexes, respectively.

Characterization of latexes

Monomer conversion. This was measured by gas-phase chromatography (Supelco phase 19 GS) with Intersmat IGC 112F equipment, using on-line analysis[17]. Sampling was carried out all along the polymerization in order to determine the solids content and particle size.

Copolymer composition. The copolymer composition of the various samples at different conversions was

Table 1

Emulsifier	Structure	Water solubility (g/100 ml) at 30°C	C.m.c. ($g l^{-1}$)	Molecular surface area ($Å^2$/molecule)
MA80	$CH_2COOC_6H_{13}$ | $CH—COOC_6H_{13}$ | $SO_3^-Na^+$	34.0	1.0	39 (desorption)[a] 45 (adsorption)
N22	$CH_2—COONa$ | $CH—COONa$ | $N—C_{18}H_{37}$ | CH_2 | $CH—COONa$ | $SO_3^-Na^+$	∞	0.06	41[a]

[a] Data provided by the supplier

deduced from ^{1}H n.m.r. spectra carried out with a Bruker CW80 spectrometer on 5 wt% solutions in deuterated chloroform. The sequence distribution of copolymers was determined from ^{13}C n.m.r. spectra at 120°C recorded with a Bruker WP 80 spectrometer on 15–20 wt% sample solutions in $CDCl_3$. Details on the operating procedure and calibration are provided in a previous paper[18].

Molecular weights. These were determined by g.p.c. in tetrahydrofuran (THF) solutions using microstyragel columns and polystyrene standards.

Glass transition temperatures. The T_g of copolymers were determined with DSC-110 Setaram equipment between −100°C and 130°C, using a heating rate of 10°C min^{-1}.

Particle size and particle size distribution. These were determined using either dynamic light scattering methods (Coulter Nanosizer from Coultronics or Malvern equipment) or transmission electron microscopy (Philips EM300) using a cold stage and negative staining by phosphotungstic acid (PTA). Particle number was deduced from the solids content and the weight-average particle diameter.

Surface charge density. This was measured after ionic exchange on mixed-bed resins (Dowex A101D–Dowex C204) by following the conductivity upon titration with 0.02 N sodium hydroxide (and 0.02 N hydrochloric acid for back-titration), from which the type and concentration of surface acid charges were determined.

SIMULATION OF THE KINETICS AND MICROSTRUCTURE OF COPOLYMERS

Simulation programs were used in this work to derive, from knowledge of the overall polymerization rate (solid contents and g.c. analysis) and rate of addition of monomers, the rate of consumption of any monomer, the main and instantaneous copolymer composition, as well as the microstructure (sequence distribution) of these copolymer chains as a function of reaction time. In addition, as developed elsewhere[19], it is also possible to compute a theoretical glass transition temperature (T_g) behaviour of the resulting copolymers at any conversion, and one can expect to obtain useful information from the comparison of theoretical and experimental d.s.c. curves. In the same way, knowledge of theoretical microstructure and its change as a function of conversion or process is necessary to get safe data from n.m.r. analysis of the copolymers and, finally, to correlate better with mechanical properties of corresponding films.

Given that the main objective is the study of the copolymer, the simulation used in this work does not take into account nucleation and it is based on monomer partition coefficients between the aqueous and organic phases and not on a more sophisticated thermodynamic approach[20]. The main parameters used are summed up in *Table 2*.

The simulation also takes into consideration the existence of polymerization in the water phase along with polymerization within the particles. However, owing to the rather low water solubility of both monomers and to their relatively low propagation rate constants, the copolymer generated in the water phase is practically negligible.

Except for batch copolymeization, in all processes, monomers are fed at a given rate, so it is necessary to consider the competition between the rate of polymerization (R_p) and the rate of monomer addition (R_a), which determines the rate of monomer accumulation, and, as a consequence, the complexity of the mixture of copolymer chains, closely related to the monomer composition drift allowed by the process. It is, thus, practicable to feed the computer with the profile of the overall polymerization rate (from solids content measurements, for instance) *versus* conversion and with the feeding rate of each monomer. The program computes the overall propagation rate constant, which is a complex function of homopolymer k_p values, reactivity ratios and instantaneous monomer composition[21]. All useful functions are calculated—instantaneous and mean values—and plotted vs. time or overall conversion. Theoretical thermograms (d.s.c.) are also derived at various conversions, which can be compared with experimental data. In the same way, the sequence distribution functions (dyads, monomer centred in the different triads,...) are computed vs. conversion.

RESULTS AND DISCUSSION

Polymerization recipes of the PS seed latex and of the various (S–BuA) copolymer latexes are described in *Tables 3* and *4*, respectively. As required to obtain small particle size so as to provide enough emulsifier coverage for the seed copolymerization reactions, high emulsifier concentration was chosen; this results in a not too broad PS seed particle size distribution ($D_w/D_n \sim 1.10$).

Reactivity ratios of the binary system in the presence of an Aerosol MA80–Aerosol N22 emulsifier mixture were determined using composition analysis of low-conversion copolymers (< 10%), for various comonomer feed compositions; classical methods were applied to calculate the following reactivity ratios: $r_S = 0.71 \pm 0.05$

Table 2 Simulation main parameters

	Styrene	Butyl acrylate
Partition coefficients, $K = [M]_w/[M]_o$	0.002	0.005
Maximum swelling of latex particle, M_p/P	1.88	1.88
Propagation rate constant, k_p (l mol^{-1} s^{-1})	350	200
Termination rate constant, k_t (l mol^{-1} s^{-1})	10^3	10^6
Homopolymer T_g (°C)	105	−52
Reactivity ratio, r_{ij}	0.71	0.21

Table 3 PS seed recipe and TEM characterization

Ingredient	Parts by weight (g)
DI water	900
Styrene	100
MA80	36
N22	7
$K_2S_2O_8$	0.6
$NaHCO_3$	0.6
D_n	48
D_w	53
D_w/D_n	1.1

and $r_{BuA} = 0.21 \pm 0.05$. These values are in good agreement with those recently determined in different laboratories[2,3] with sodium dodecylsulphate (SDS) or soapless conditions, respectively. The results indicate that the S/BuA partition between water, droplets and swollen particles is not strongly affected by the concentration or type of emulsifier, probably because of the low aqueous solubility of both monomers.

Homogeneous copolymerization

In batch reactors, because of the differences in reactivity ratios, one can expect to have a continuous drift of the copolymer composition, with S-rich copolymer chains formed at low conversion and BuA-rich macromolecules at the final stage. Therefore, the composition-controlled process (CC) was used in order to prepare quite homogeneous copolymer particles by on-line keeping constant the unreacted monomer ratio into the reactor, as has already been described. This can be observed in *Figure 1* for three compositions (25, 50, 70 mol% BuA).

All conversion–time curves exhibit the three classical intervals observed in batch processes (nucleation, constant rate and decreasing rate), which seems to be logical since in these CC most of the total amount of monomers is added before starting the reaction (see *Table 3*) and only the remaining S (the more reactive monomer) is fed dropwise to avoid compositional drift. The reverse is true in the conventional semi-continuous (or semi-batch) process where only a part of the total monomers (10–20%) is added at the beginning, the remainder being fed dropwise all along the process.

Figure 1a shows the variations of the overall conversion (X_{global}) and the instantaneous copolymer composition ($F_{S,inst}$) respectively, as a function of time for the homogeneous copolymer (CC1). The simulations were carried out taking into account the experimental conversion data and styrene feeding conditions. Up to 20% conversion (nucleation step) the copolymerization rate was slow and the instantaneous copolymer composition was kept nearly constant. After this initial stage, the rate is highly accelerated, which causes a slight compositional drift, because the time span between two g.c. analyses of the unreacted monomers becomes meaningful before the computer set-up takes the S/BuA ratio to its initial value. In spite of these drastic conditions, this CC process is able to produce quasi-homogeneous copolymers as corroborated by ^1H n.m.r. analysis of intermediate samples (see the corresponding values on the diagram on *Figure 1a*). The same behaviour is observed for the CC2 experiment (*Figure 1b*) which also shows a slight variation of F_S vs. time when the copolymerization rate suddenly increases. Simulation of the cumulative composition and experi-

Table 4 BuA–S copolymerization recipes[a]

Code	Copolymerization process	Core		Shell		Third layer
		BuA(g)	S(g)	BuA(g)	S(g)	BuA(g)
CC1	Controlled	77	7+(16)[b]	—	—	—
CC2	Composition	55	22+(23)[b]	—	—	—
B3	Batch (azeotrope)	31	69	—	—	—
CS1	Core–shell	—	10(seed)	77	13	—
CS2		—	10(seed)	55	35	—
CS3		—	10(seed)	31	59	—
ML1	Multilayer	—	10(seed)	67	13	10
ML2		—	10(seed)	45	35	10
ML3		—	10(seed)	21	59	10

[a] Temperature, 70°C; $NaHCO_3$, 0.3 g; $K_2S_2O_8$, 0.6 g; MA80, 3.6 g; 22N, 0.7 g; DI H_2O, variable; monomer feed rate, 6 g h^{-1}
[b] Programmed addition of S in CC processes

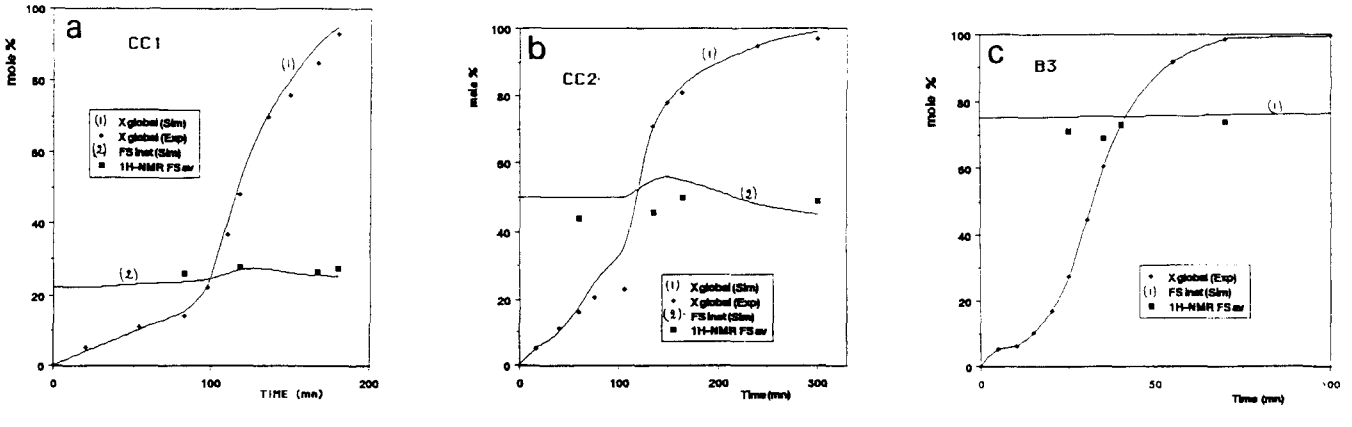

Figure 1 Composition-controlled S–BuA emulsion copolymerization. Simulation of the overall conversion X_{global} (mol%) and instantaneous copolymer composition $F_{S,inst}$ vs. time (a) CCl (S/BuA = 75/25; (b) CC2 (S/BuA = 50/50); (c) B3 (S/BuA = 25/75)

mental data (from ^{1}H n.m.r.) are in good agreement, and the equimolecular composition is obtained.

For this binary system, since both r_{ij} values are <1, an azeotropic feed composition according to the polymerization equation, with $S/BuA=(1-r_2)/(1-r_1)=2.72$, would be expected. Such a composition was chosen for experiment B3, so that it was not necessary to use the controlled process. The comparison between experimental data and instantaneous and cumulative simulation curves does not exhibit any compositional heterogeneity (*Figure 1c*). A faster copolymerization rate than in CC1 and CC2 experiments due to a higher initial monomer concentration (all ingredients, including monomers, were indeed charged before starting the reaction) was observed. It is also interesting to note (*Figure 2*) that the average particle number N_p becomes practically constant at nearly 15% conversion, which indicates that for this S-rich composition, no continuous nucleation occurs during particle growth.

Core–shell copolymerization

It is well known that the rate of polymerization and the morphology of latex particles can be affected by many reaction variables; when dealing with semi-batch, two of them are the feed rate of the shell monomers and the control of particle nucleation (no new crop is generally desired). In the present study, since the PS seed was fully covered by the emulsifier, no secondary nucleation should occur. Polymerization conditions for these core–shell process (CS) are summarized in *Table 3*. A very low feed rate ($R_a=6\,g\,h^{-1}$) was chosen to promote surface polymerization and consequently core–shell structures. High instantaneous conversions were obtained for both monomers as shown in *Figure 3* for runs CS1, CS2 and CS3. Under these conditions, particle swelling was minimized; thus, monomers and macroradicals within particle cores would appear unlikely. In such a process, polymer transfer reactions (grafting) might be promoted due to the high polymer/monomer ratio. Although such reactions are more probable in the reverse situation[13], it is expected that the graft copolymer, if any, would be distributed at the interface of the PS seed/PS(S–BuA) shell, thus contributing to the stabilization of macromolecular domains in each particle.

Predicted instantaneous copolymer composition–time curves (mol% S) reach a steady-state plateau at low conversion (18% for CS1 (*Figure 3*)*a*, 48% for CS2 (*Figure 3b*) and about 70% for CS3 (*Figure 3c*)). It should be noted that cumulative copolymer composition curves have no direct physical meaning since the polymer constituting the core (PS) is not the same as the one forming the shell (PBu–S).

Owing to a favourable r_{ij} for styrene, simulated instantaneous S conversion (X_S) seems to be higher than for BuA. However, experimental kinetic data and final average copolymer composition (from ^{1}H n.m.r.) agree quite well with model predictions.

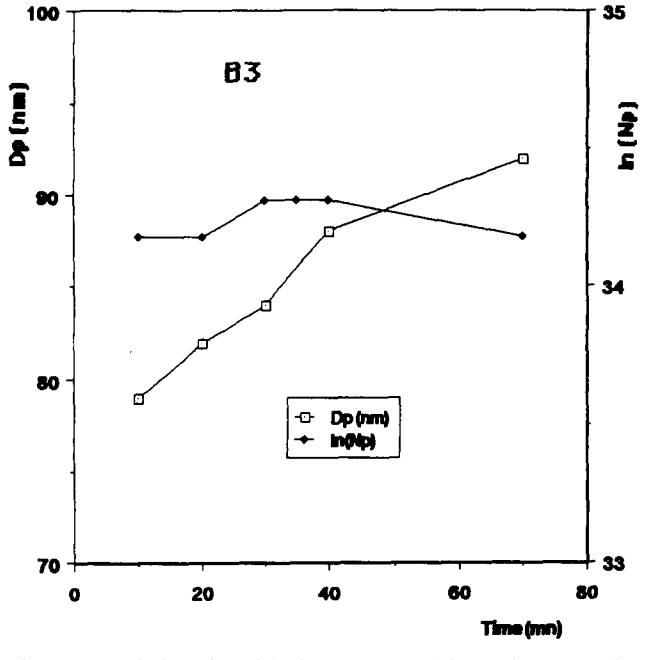

Figure 2 Variation of particle size D_p and particle number N_p vs. time for run B3

Multistep polymerization

Keeping the same overall copolymer composition (25, 50 and 70 mol% BuA, respectively) a series of latexes were prepared using a three-stage polymerization process (MS), as already described in the 'Experimental' part. Such latexes were aimed at investigating the effect of an intermediate shell on the mechanical properties of films originated from them. This was done by direct comparison of these properties with those of the films obtained from homogeneous latexes. PS and PBuA homopolymers not being compatible, it is expected that

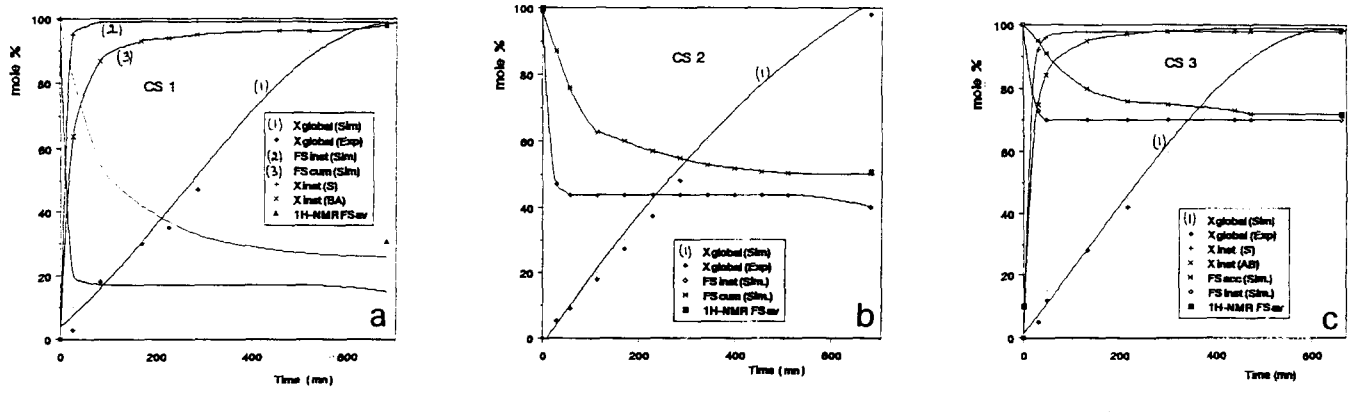

Figure 3 Core–Shell S–BuA emulsion copolymerization. Simulation of the overall conversion X_{global} (mol%), and instantaneous ($F_{S,inst}$) and cumulative ($F_{S,cum}$) copolymer compositions. (a) CS1 (S/BuA = 75/25): (b) CS2 (S/BuA = 50/50); (c) CS3 (S/BuA = 25/75)

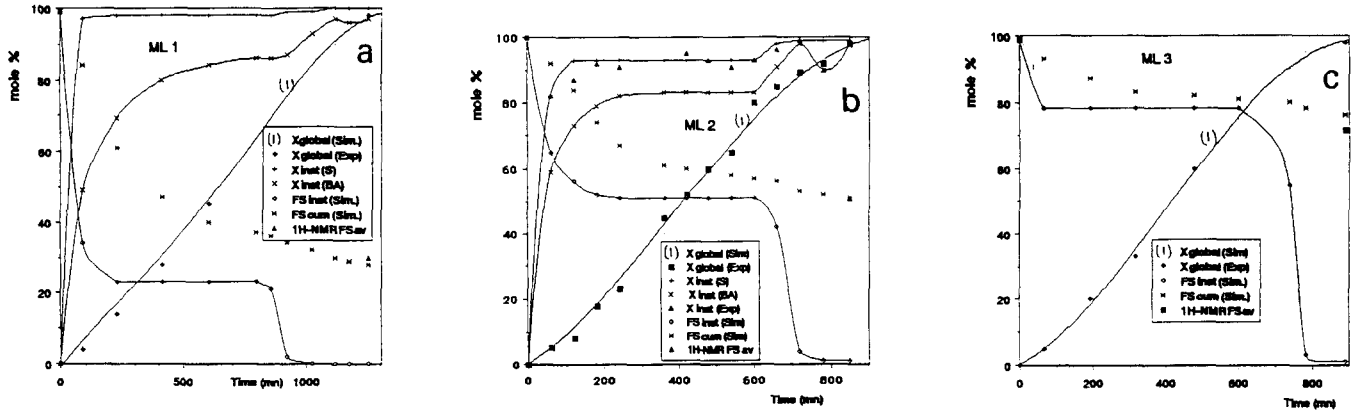

Figure 4 Multistage S–BuA emulsion copolymerization. Simulation of the overall conversion X_{global} (mol%), and instananeous ($F_{S,inst}$) and cumulative ($F_{S,cum}$) copolymer compositions. (a) ML1 (S/BuA = 75/25): (b) ML2 (S/BuA = 50/50); (c) ML3 (S/BuA = 25/75)

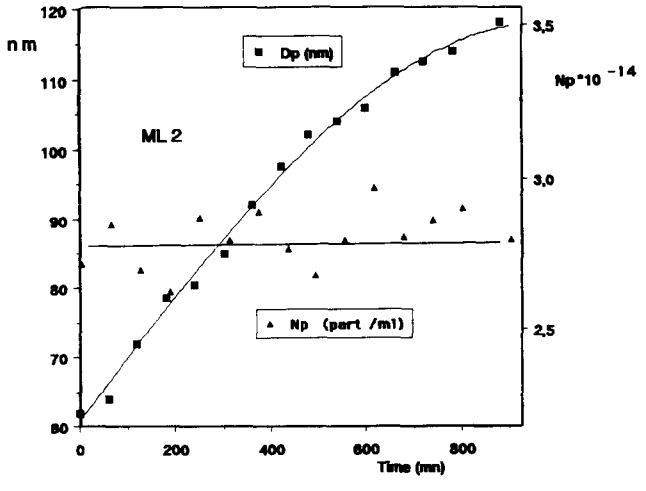

Figure 5 Variation of particle size D_p and particle number N_p vs. time for run ML2

the incorporation of an intermediate layer of S–BuA copolymer at the interface would favour the interactions between the various polymer phases, thus reducing the phase rearrangement, mainly during film formation[16]. As already stated, any grafting reaction can also improve the stabilization of these domains in the composite particles.

Simulation curves, reported in *Figure 4*, suggest a quite high instantaneous conversion for both monomers, particularly for S. The evolution of the instantaneous copolymer compositions vs. time exhibits three typical periods. Initially, PS seed is the only dispersed phase ($F_S = 1.0$), then a homogeneous copolymer constituted second layer is produced, the composition of which depends on the overall monomer composition, in any case. Finally, pure BuA is polymerized ($F_S = 0.0$). The average composition values (from ^{1}H n.m.r.) of the final copolymers agree quite well with the corresponding predicted ones. In relation to the particle size and particle number variation as a function of time, experimental data (*Figure 5* from run ML2) show a continuous increase in D_p as a function of reaction time; the particle number is, then, being kept practically constant all along the process. Generally, no new secondary crop of particles was found for these multistep polymerizations.

In conclusion, computer modelling based upon gravimetric analysis (overall conversion) and monomer feeding policies, fed on-line to the simulation program, allows one to predict satisfactorily complex emulsion processes, like those carried out to synthesize core–shell or multilayer composite particles.

MOLECULAR PROPERTIES OF COPOLYMERS

Molecular weight and molecular-weight distribution

It is well known that the monomer composition affects the copolymer microstructure as well as the molecular weight and molecular-weight distribution[22,23]. Furthermore, under emulsion conditions, it has been shown that the reaction pathway strongly influences the *MWD*. These two parameters have to be considered in order to explain the experimental results (M_w, M_n, M_w/M_n) given in *Table 5* for all samples.

Although M_w and M_n are not absolute values, they are useful for comparison. Mark–Houwink constants are indeed necessary to derive these absolute values from the universal calibration method applied to the g.p.c. chromatograms. Since such constants are not known for BuA–S copolymers, the measured M_w values are related, only, to PS standards.

For the discussion of the data, it will be assumed, for the sake of simplicity, that the general expression of DP_n (average degree of polymerization) is applicable to copolymerization reactions. If chain transfer occurs, then DP_n is given by:

$$DP_n = \frac{R_p}{R_t + \sum R_{tr}} = \frac{\bar{n} N_p k_p [M]_p / N_a}{R_{i,eff} + \sum R_{tr}}$$

where R_p is the copolymerization rate, R_{tr} is the transfer rate (to monomer or polymer), $R_{i,eff}$ is the effective intiation rate, R_t is the termination rate, k_p is the average propagation rate constant, $[M]_p$ is the overall monomer concentration in polymer particles, N_A is Avogadro's number and $\bar{n}$ is the average number of free radicals per particle.

Since initiator concentrations and polymerization temperatures were practically the same for all experiments, it is obvious that the observed differences in molecular weight (*Table 5*) are mainly dependent upon three factors: the monomer concentration into the polymer particles ($[M]_p$), the average number of free

Table 5 Molecular-weight characteristics

Code	Composition via ^{1}H n.m.r. (mol% BuA)	Type of process	M_w ($\times 10^{-3}$)	M_n ($\times 10^{-3}$)	M_w/M_n
PS seed	—	Batch	1204	362	3.3
CC1	72.0	Controlled	2435	716	3.4
CC2	50.0	composition	1305	241	5.4
B3	24.7	Batch (azeotrope)	1726	384	4.5
CS1	68.6	Core–shell	402	35	11.6
CS2	48.9		835	69	12.1
CS3	28.0		885	112	7.9
ML1	70.0	Multilayer	467	44	10.6
ML2	50.5		630	113	5.5
ML3	28.6		858	115	7.4

radicals/particle ($\bar{n}$) and the extent of transfer reactions (R_t). These factors vary according to the reaction pathway and monomer feed composition.

As for the effect of the monomer addition mode, it should be recalled that in batch copolymerization both monomers are totally charged into the reactor from the very beginning, whereas in multistage polymerization low feeding rates ($< R_{p,max}$) make the system reach a steady state (*Figures 3–5*) which results in a very low amount of unreacted monomers during the process. The controlled copolymerization process can be considered as an intermediate between the batch and semi-continuous processes, at least as far as monomer concentration within the particles during reaction is concerned. It can be seen from *Table 5* that azeotropic batch (B3) and controlled copolymerizations (CC1, CC2) lead to higher M_w than do multistage polymerizations (CS and ML series), which can be explained by the difference in [M] in the reaction loci, regardless of the monomer composition in the feed:

$$[M]_p(B) > [M]_p(CC) > [M]_p(ML \text{ and } CS)$$

Therefore:

$$M_w(B) > M_w(CC) > M_w(ML \text{ and } CS)$$

Moreover, it is clear that polydispersity ratios increase from batch polymers (PS seed and B3), which are mainly formed by one product, to core–shell and multilayer polymers, which are composed of different molecular-weight species; for instance, ML composites contain three different molecular-weight polymers coming from the PS seed, copolymer intermediate layer and PBuA final layer. It is also clear that surface polymerization, as has already been noted[12], plays a dominant role in the latter process. This polydispersity index is not strongly modified by the monomer composition.

In relation to the effect of monomer composition, the results obtained will be discussed according to the type of process. In both batch and CC processes, the presence of monomer droplets up to 40–50% conversion permits the polymer particles to keep a maximum swelling ratio for a long polymerization time; therefore similar trends should be observed. It has recently been shown that M_w tends to increase when increasing the BuA proportion, either under soap-free emulsifier[2] or SDS emulsified conditions[3]; we made the same observation here for the PS seed and BuA-rich controlled copolymer (BC1). If the propagation rate constants are relatively similar for both homopolymers, the reverse is true for termination rate constants (*Table 2*), where $k_t(S) \gg k_t(BuA)$; this means that by increasing the BuA proportion the cross-termination rate constant (k_{t12} for copolymerization) decreases, and therefore the possibility of having more than one radical per particle increases, giving higher M_w.

In the case of multistage polymerizations, the variation of M_w with monomer composition exhibits a surprising behaviour, since the reverse tendency is observed in comparison with that obtained in the case of batch processes. As previously discussed, instantaneous free monomer is quite low in semi-continuous processes (starved conditions), and hence Tromsdorff's gel effect and transfer reactions to polymer cannot be discarded. In that case, the average cross-termination rate constant, k_{t12}, becomes diffusion-controlled, and is then dependent on the molecular mass of both the diffusing growing chains and the copolymer forming the particles. The diffusion coefficient is inversely proportional to the frictional parameter, which in turn is directly proportional to the viscosity of the medium. It seems that when the S content in the copolymer is increased, the viscosity of the particle increases also, since the glass transition temperature becomes higher; this involves a lower termination rate constant which results in a higher M_w (and possibly a higher average number of radicals per particle). In any case, the variation of T_g as a function of S in the copolymer might be partially or totally responsible for the increase in M_w observed in CS and ML copolymers.

Furthermore, concerning the occurrence of transfer reactions onto the pre-existing polymer, it appears from previously published work[13] that S-ended macroradicals would be more reactive than BuA ones. This effect could also contribute to enhancing the M_w when increasing the S proportion in the copolymer. Moreover, since termination mainly proceeds by coupling in S polymerization, that will increase the effect if transfer reactions are considered. However, owing to the complexity of such a system, it is difficult to discriminate the contribution of each effect.

Table 6 Compositional triad distributions[a]

Code	Composition via ^{1}H n.m.r. (mol% BuA)	S-centred triads			BuA-centred triads		
		S–S–S	S–S–BuA	BuA–S–BuA	S–BuA–S	S–BuA–BuA	BuA–BuA–BuA
CC1	72	— (0.004)	0.18 (0.118)	0.82 (0.880)	0.16 (0.103)	0.36 (0.435)	0.48 (0.462)
CC2	50	0.07 (0.105)	0.33 (0.437)	0.60 (0.458)	0.54 (0.588)	0.33 (0.358)	0.13 (0.055)
B3	24.7	0.44 (0.483)	0.46 (0.424)	0.10 (0.092)	0.85 (0.885)	0.15 (0.110)	— (0.005)
CS1	68.6	0.44 (0.369)	0.17 (0.133)	0.39 (0.497)	0.13 (0.047)	0.37 (0.338)	0.50 (0.614)
CS2	48.6	0.34 (0.241)	0.27 (0.288)	0.39 (0.477)	0.39 (0.394)	0.45 (0.454)	0.16 (0.152)
CS3	28.0	0.45 (0.461)	0.41 (0.410)	0.14 (0.129)	0.74 (0.838)	0.26 (0.155)	— (0.007)
ML1	70.0	0.46 (0.454)	0.10 (0.096)	0.44 (0.449)	0.10 (0.197)	0.30 (0.278)	0.60 (0.524)
ML2	50.5	0.29 (0.312)	0.32 (0.206)	0.39 (0.48)	0.43 (0.547)	0.33 (0.198)	0.24 (0.252)
ML3	28.6	0.64 (0.718)	0.30 (0.220)	0.06 (0.062)	0.64 (0.640)	0.16 (0.030)	0.20 (0.322)

[a] ^{13}C n.m.r. experimental data (simulation predicted values in parenthesis)

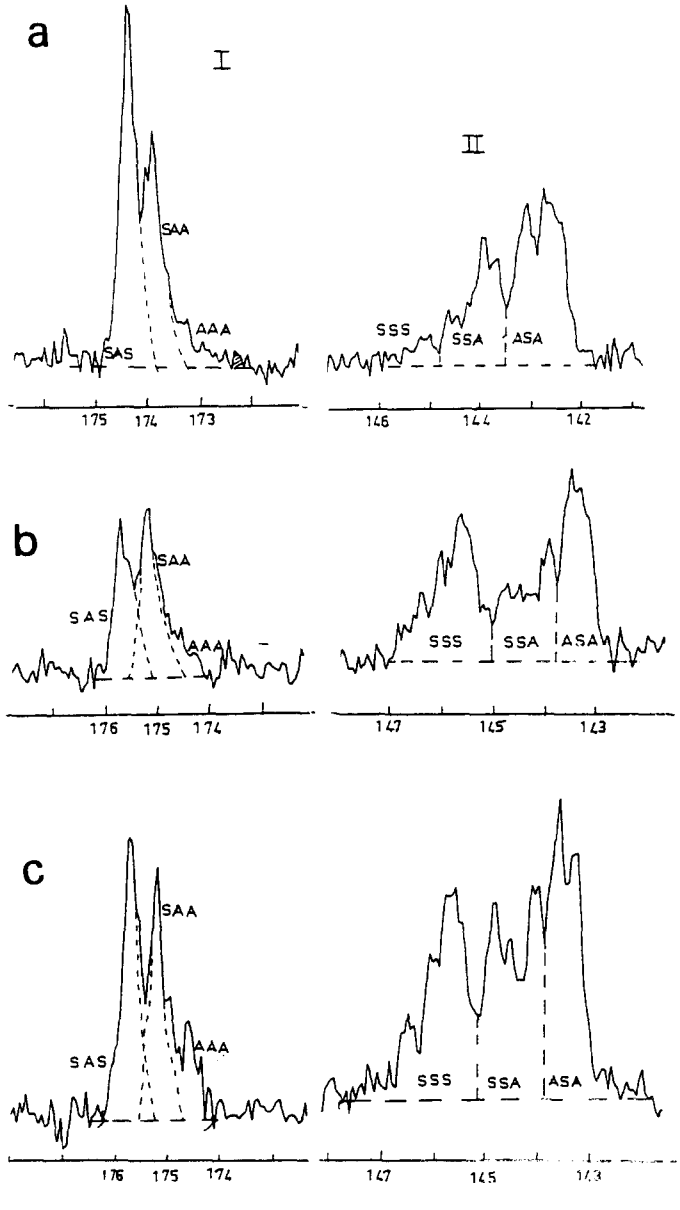

Figure 6 Expanded spectra (20.1 MHz) of the carbonyl carbon (BuA) (I) and C1 (S) (II) resonance region of a styrene–n–butyl acrylate copolymer (S/BuA = 50/50), prepared through (a) composition-controlled, (b) core–shell and (c) multistage emulsion copolymerization processes, respectively

Microstructure of copolymers

The knowledge of the microstructure of copolymers is a key factor for investigating structure–property relationships. All copolymers were characterized in terms of sequence distribution through a ^{13}C n.m.r. analysis[18] based on an earlier work in which the assignment of the various ^{13}C resonance peaks was done. It was clearly shown that due to the difference in reactivity ratios, significant discrepancies were exhibited between batch and semi-continuous copolymers.

In *Table 6*, the average copolymer compositions of the various copolymers together with the S- and BuA-centred triad proportions are summarized. Expanded spectra of the BuA carbonyl (C=O) and S quaternary carbon (C1) resonance regions for 50 mol% copolymers are reported in *Figure 6*.

The theoretical approach for calculating the sequence distribution has already been described elsewhere[18]. Through a numerical integration procedure that takes conversion into account, monomer partition between the various phases, and instantaneous and cumulative monomer sequence distributions, can be simulated. In the case of structured copolymers (CS and ML), it should be noted that the simulation program computes the microstructure evolution all along the different reaction stages; thus, the values reported in *Table 6* are the accumulated ones at the end of the process, as a function of the monomer composition of the corresponding steps. Generally, a good agreement is observed between the predicted values and the experimental data, except maybe in the case of S-rich copolymers where high overlapping of the three S-centred triad peaks causes less accuracy in the evaluation by planimetry.

As expected, core–shell and multilayer copolymers display higher S–S–S triad proportions than the homogeneous ones since the former were produced by seed copolymerization in the presence of 10 wt% PS seed (see for example CS1, ML1 and B3 in *Table 6*). Moreover, owing to the nature of the CC process, compositional drift is avoided, thus the formation of long S (or BuA) sequences is eliminated. Hence, sequence distribution differences in those three copolymers are particularly important. It is noteworthy that, in the case of multilayer copolymers where a layer of pure PBuA (10 wt%) was produced in the last stage, the BuA–BuA–BuA triad

Table 7 Glass transition temperatures (°C)[a]

Code	Composition (mol% BuA)	T_{g1} (PBuA)	T_{g2} (Copolymer)	T_{g3} (PS)
PS seed	0.0			102 (105)
PBuA	100	−54 (−55)		
CC1	72.0		−36 (−24)	
CC2	50.0		13 (8)	
B3	24.7		55 (45)	
CS1	68.6		−31 (−33)	106 (105)
CS2	48.6		3 (−4)	106 (105)
CS3	28.0		45 (37)	106 (105)
ML1	70.0	−55 (−55)	−30 (−30)	103 (105)
ML2	50.5	−57 (−55)	3 (2)	103 (105)
ML3	28.6	−54 (−55)	53 (50)	103 (105)

[a] D.s.c. experimental data (simulation predicted values in parentheses)

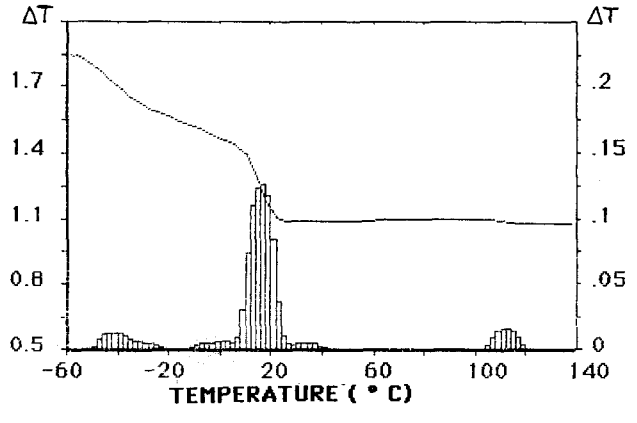

Figure 7 Simulation (I) of the thermogram curve (d.s.c.) and glass transition temperature histogram for sample CS2

proportion is clearly found to increase regardless of the initial monomer feed composition. All this means that ^{13}C n.m.r. analysis of such BuA–S composites is precise enough to discriminate the effect of the reaction pathway on the sequence distribution in a large monomer composition range.

Glass transition temperature

Experimental data and computer predicted values of the glass transition temperature are reported in *Table 7* for the different S–BuA copolymers. The simulation program gives, whatever the polymerization process may be, the microstructure of the macromolecules instantaneously generated and their corresponding T_g values according to Johnston's equation[24], as a function of time or conversion. Thus, a theoretical histogram (weight T_g distribution) is obtained from which the mean glass transition temperature is computed[19], as shown in *Figure 7* for sample CS2.

The simulation gives a quite good description of the experimental results. Homogeneous copolymers (CC1, CC2 and B3) show only one T_g, as expected, with a limited glass transition region owing to the small composition drift allowed by the polymerization process. Core–shell and multilayer copolymers show two and three T_g values respectively, depending on the composition of each polymerization step. No change was observed on the glass transition region of PS and PBuA domains, which indicates that intermolecular interactions between the different polymer regions are not important (very low compatibility), even in the presence of an intermediate copolymer layer, whose composition does not appear to be significant. This means that the monomer sequence distribution (microstructure), which affects the chain flexibility, determines the glass transition temperature behaviour for these S–BuA structured copolymers.

COLLOIDAL CHARACTERISTICS OF LATEXES

The different latexes have been characterized in terms of particle size and surface properties as reported in *Tables 8* and *9*, respectively. Concerning the particle size, two methods were used, dynamic light scattering (DLS) and transmission electronic microscopy (TEM), from which the particle size distribution and particle number have been evaluated. Some discrepancy is clearly shown according to the method, the lower values obtained by TEM probably being caused by the shrinkage of the particles under the electron beam. As expected, the seed PS latex exhibits a low particle size with a slightly broad distribution. CC latexes display a particle size decreasing with increasing S content; surprisingly the B3 sample, which was prepared without the CC process, appears to be more polydisperse. It is found that the CS and ML latex series show particle sizes relatively near the theoretical values (if the calculation is based on DLS data). Such a trend is confirmed when considering particle numbers in the last two columns of *Table 8*. Slightly higher values for final N_p (compared to initial N_p), as observed in CS1, CS2 and ML1 samples, suggest that some secondary crop of particles could be formed during the synthesis.

Concerning the surface properties (*Table 9*), two types of end-groups have been identified and quantified: sulphate (SO_4^-) and carboxylic (COO^-) groups. While the former groups result from the decomposition of the initiator ($K_2S_2O_8$) and the subsequent incorporation of the water-phase-originated oligomers onto the particles, some uncertainty may arise about the latter ones. Indeed, the presence of carboxylic groups, at the interphase could result from three different mechanisms; (i) Hydrolysis and oxidation of sulphate end-groups during synthesis or upon ageing; however, such a reaction (so-called Kolthoff reaction[25]) was shown to be operative at low pH, and under the actual polymerization conditions, the aqueous phase has been buffered with sodium hydrogen carbonate (pH ~ 8). (ii) Hydrolysis of surface-exposed BuA units; this reaction, even though it cannot be discarded, is found to proceed more likely above pH 9. Furthermore, the concentration of COOH is not seen to be increased in BuA-rich latexes. (iii) Emulsifier molecules either by simple adsorption or more probably by transfer reaction to a labile hydrogen: although there is no direct evidence of such transfer, this reaction would concern the Aerosol 22N molecular for which there are three COO^- attached groups (see *Table 1* for the structure of surfactants) per one grafted molecule. Accordingly, some SO_3^- groups would also be incorporated; however, they cannot be distinguished from the SO_4^- groups in the titration curve.

The occurrence of the grafting reaction can be well corroborated when considering the surface charge

Table 8 Particle size determinations by DLS and TEM

Code	Composition via ^{1}H n.m.r. (mol% BuA)	DLS	TEM			Theoretical	N_{p0}	N_{pf}
		D_p(nm)	D_n(nm)	D_w(nm)	D_w/D_n	D_{pf}(nm)	($\times 10^{-14}$)	($\times 10^{-14}$)
PS seed	—	60	48	53	1.10	—	—	—
CC1	72.0	93	85	91	1.07	—	—	5.3
CC2	50.0	97	75	79	1.05	—	—	8.72
B3	24.7	—	60	69	1.15	—	—	16.57
CS1	68.6	99	84	89	1.05	102	4.37	4.66
CS2	48.6	98	—	—	—	104	4.37	4.96
CS3	28.0	110	—	—	—	108	3.21	3.19
ML1	70.0	104	81	92	1.13	108	3.02	3.57
ML2	50.5	110	83	89	1.05	109	3.02	2.98
ML3	28.6	117	108	113	1.04	109	3.02	2.87

Table 9 Surface characterization of cleaned latexes

(μ Eq g^{-1} polymer)	End-group (μE/g polymer)		Charge density (Å^2/molecule)				
Code	SO_4^-	COO^-	SO_4^-	COO^-	Global	M_n ($\times 10^{-3}$)	SO_4^-/chain
PS seed	7.30	16.4	—	—	—	362	2.64
CC1	—	—	—	—	—	—	—
CC2	1.96	9.86	4944	982	820	241	0.47
B3	2.26	11.32	4201	838	699	384	0.87
CS1	8.79	18.20	1080	521	331	35	0.31
CS2	5.05	16.80	1899	570	438	69	0.35
CS3	7.07	16.68	1329	563	359	112	0.79
ML1	10.78	18.58	838	486	307	44	0.47
ML2	7.80	13.07	1095	653	425	113	0.88
ML3	8.64	—	989	—	989	115	0.99

densities of the PS seed latex (for which the same recipe as for the other latexes was used). The average number of SO_4^- per polymer chain (as determined from the M_w data), i.e. 2.64, is higher than the theoretical value of 2 expected for PS (assuming that coupling termination is predominant).

In the CC and batch latexes, the SO_4^- density is much smaller ($\sim 2\,\mu E\,g^{-1}$ polymer) and the average number of SO_4^- per molecule seems to decrease with increasing BuA content in the monomer feed; the COO^- charge density is also smaller, but still high. In the CS and ML latexes the production of low molecular weight causes the SO_4^- charge density to be increased; however the average number of SO_4^- per macromolecule is of the same order as in the batch series and the same tendency is to be noted, as a function of the monomer feed composition. For all the latexes, the COOH concentration is always significant, which is indicative that the grafting reaction of the emulsifier (Aerosol 22N) onto the polymer particles is probably enhanced due to the nature of the process (where surface polymerization is favoured).

CONCLUSIONS

In conclusion, butyl acrylate–styrene copolymer latexes exhibiting various compositions and differences in molecular and colloidal properties can be prepared through emulsion copolymerization thanks to the versatility of the emulsion process. Simulation programs, based upon available parameters (reactivity ratios, partition coefficients, etc.), and upon given 'on-line data', were found to be well adapted in predicting the kinetics of the various emulsion copolymerizations, as well as the microstructure and thermal behaviour of the corresponding copolymers. Such well characterized latexes can be considered as models, suitable for the investigation of structure–property relationships, as will be shown for the viscoelastic behaviour of the films derived from these latexes, in the second part of this series.

REFERENCES

1 Mangaraj, D. and Roth, B. *Prepr. ACS Div. Polym. Chem.* 1972, **13**(1), 349

2 Guillaume, J. L., Pichot, C. and Revillon, A. *Makromol. Chem. Suppl.* 1985, **10/11**, 69
3 Cruz, M. A., Palacios, J., Garcia-Rejon, G. A., Ruiz, L. M. and Rios, G. L. *Makromol. Chem. Suppl.* 1985, **10/11**, 87
4 Rohm & Haas in 'Encyclopedia of Polymer Science and Technology', Interscience, New York, vol. 1, 246, 1964
5 Hamaide, T., Revillon, A. and Guyot, A. *Eur. Polym. J.* 1984, **20**, 855
6 Snuparek, J. *Appl. Polym. Sci.* 1977, **21**, 2253
7 Barton, J. *Acta Polym.* 1985, **36**(4), 187
8 Basset, D. R. in 'Science and Technology of Polymer Colloids', (Eds. G. W. Poehlein, R. W. Ottewill and J. W. Goodwin), NATO Series Appl. Sci. 67, 1983
9 Daniel, J. C. *Makromol. Chem. Suppl.* 1985, **10/11**, 24
10 Matsumoto, T., Okubo, M. and Imai, T. *Kobunshi R.* 1974, **31**(9), 576; Eng. Transl. 1974, **3**(9), 1814
11 Okubo, M., Yamada, A. and Matsumoto, T. *J. Polym. Sci., Polym. Chem. Edn.* 1980, **16**, 3219
12 Stutman, D. R., Klein, A. El Aasser, M. S. and Vanderhoff, J.W. *Ind. Eng. Chem. Prod. Res. Dev.* 1985, **24**(3), 404
13 Min, T. I., Klein, A., El Aasser, M. S. and Vanderhoff, J. W. *J. Polym. Sci., Polym. Chem. Edn.* 1983, **21**, 2845
14 Cavaille, J. Y., Jourdan, C., Kong, X. Z., Perez, J., Pichot, C. and Guillot, J. *Polymer* 1986, **27**, 693
15 Dimonie, V., El Aasser, M. S., Klein, A. and Vanderhoff, J. W. *J. Polym. Sci., Polym. Chem. Edn.* 1984, **22** 2197
16 O'Connor, K. J. *Appl. Polym. Sci.* 1987, **33**, 2007
17 Guyot, A., Pichot, C., Guillot, J. and Rios, G. L. *ACS Symp. Ser.* 1981, **165**(26), 415
18 Llauro-Darricades, M. F., Pichot, C., Guillot, J., Rios, G. L., Cruz, M. A. and Guzman, C. *Polymer* 1986, **27**, 889
19 Guillot, J. European Symp. on Polymer Materials, Preprints, 1987
20 Guillot, J. *Makromol. Chem.* 1982, **183**, 625
21 Djekhaba, S., Graillat, C. and Guillot, J. *Eur. Polym. J.* 1988, **24**(2), 109
22 Hamielec, A. and Friis, N. *J. Appl. Polym. Sci.* 1975, **19**, 97
23 El Aasser, M. S., Magawinata, T., Vanderhoff, J. W. and Pichot, C. *J. Polym. Sci., Polym. Chem. Edn.* 1983, **21**, 2363
24 Johnston, N. *ACS Polym. Prepr.* 1973, **14**, 46
25 Kolthoff, J. M. and Miller, I. K. *J. Am. Chem. Soc.* 1951, **73**, 3055